journal of the mechanical behavior of biomedical materials 158 (2024) 106681

Contents lists available at ScienceDirect

Journal of the Mechanical Behavior of Biomedical Materials

journal homepage: www.elsevier.com/locate/jmbbm

Computational biomechanical study on hybrid implant materials for the femoral component of total knee replacements

Jan-Oliver Sass [a,*], Maeruan Kebbach [a], Cornelia Lork [b], Jan Johannsen [c], Markus Weinmann [d], Melanie Stenzel [d], Rainer Bader [a]

[a] Research Laboratory for Biomechanics and Implant Technology, Department of Orthopedics, Rostock University Medical Center, Doberaner Straße 142, D-18057 Rostock, Germany
[b] ZM Praezisionsdentaltechnik GmbH, Breite Straße 16, D-18055 Rostock, Germany
[c] Fraunhofer Research Institution for Additive Manufacturing Technologies IAPT, Am Schleusengraben 14, D-21029 Hamburg, Germany
[d] TANIOBIS GmbH, Im Schleeke 87-91, D-38642 Goslar, Germany

ARTICLE INFO

Keywords:
Total knee replacement
Femoral component
Implant material
Beta titanium
Alumina-toughened zirconia ceramic
Uncemented fixation
Bone-implant interaction
Stress shielding
Finite element analysis

ABSTRACT

Multifunctional materials have been described to meet the diverse requirements of implant materials for femoral components of uncemented total knee replacements. These materials aim to combine the high wear and corrosion resistance of oxide ceramics at the joint surfaces with the osteogenic potential of titanium alloys at the bone-implant interface. Our objective was to evaluate the biomechanical performance of hybrid material-based femoral components regarding mechanical stress within the implant during cementless implantation and stress shielding (evaluated by strain energy density) of the periprosthetic bone during two-legged squat motion using finite element modeling. The hybrid materials consisted of alumina-toughened zirconia (ATZ) ceramic joined with additively manufactured Ti–6Al–4V or Ti–35Nb–6Ta alloys. The titanium component was modeled with or without an open porous surface structure. Monolithic femoral components of ATZ ceramic or Co–28Cr–6Mo alloy were used as reference. The elasticity of the open porous surface structure was determined within experimental compression tests and was significantly higher for Ti–35Nb–6Ta compared to Ti–6Al–4V (5.2 ± 0.2 GPa vs. 8.8 ± 0.8 GPa, $p < 0.001$). During implantation, the maximum stress within the ATZ femoral component decreased from 1568.9 MPa (monolithic ATZ) to 367.6 MPa (Ti–6Al–4V/ATZ), 560.9 MPa (Ti–6Al–4V/ATZ with an open porous surface), 474.9 MPa (Ti–35Nb–6Ta/ATZ), and 648.4 MPa (Ti–35Nb–6Ta/ATZ with an open porous surface). The strain energy density increased at higher flexion angles for all models during the squat movement. At ~90° knee flexion, the strain energy density in the anterior region of the distal femur increased by 25.7 % (Ti–6Al–4V/ATZ), 70.3 % (Ti–6Al–4V/ATZ with an open porous surface), 43.7 % (Ti–35Nb–6Ta/ATZ), and 82.5% (Ti–35Nb–6Ta/ATZ with an open porous surface) compared to monolithic ATZ. Thus, the hybrid material-based femoral component decreases the intraoperative fracture risk of the ATZ part and considerably reduces the risk of stress shielding of the periprosthetic bone.

1. Introduction

Femoral components used in total knee replacement (TKR) are commonly made of cobalt-chromium-molybdenum alloy such as Co–28Cr–6Mo. The main reason for implant revisions represents aseptic loosening (Grimberg et al., 2023), which in part is caused by wear-particle-related osteolysis (Crutsen et al., 2022; Drynda et al., 2018; Jonitz-Heincke et al., 2019; Yang et al., 2015) and periprosthetic bone resorption due to bone stress shielding (Järvenpää et al., 2014; Lee et al., 2023; Mintzer et al., 1990). In this context, corrosion and wear-resistant oxide ceramics (e.g. alumina toughened zirconia (ATZ) ceramic, zirconia toughened alumina (ZTA) ceramic) have been introduced as alternative implant materials, showing good clinical results (Bergschmidt et al., 2016). However, femoral components based on oxide ceramics are prone to brittle fracture during high-impact events (Kluess et al., 2012; Krueger et al., 2014). Furthermore, they are bioinert materials allowing only contact osteogenesis but no firm osseointegration of the implant (Bedir et al., 2023). Therefore, the benefits of

* Corresponding author.
E-mail address: jan-oliver.sass@med.uni-rostock.de (J.-O. Sass).

https://doi.org/10.1016/j.jmbbm.2024.106681
Received 29 April 2024; Received in revised form 15 June 2024; Accepted 8 August 2024
Available online 10 August 2024

uncemented implantation, such as improved component fixation through direct integration with the bone, preservation of bone stock, and reduced systemic side effects associated with debris and third-body wear, cannot be realized in cemented TKR (Uivaraseanu et al., 2022). Moreover, uncemented TKRs made of oxide ceramics similar lead to stress shielding of the periprosthetic bone since there is a mismatch in elasticity of the implant material and bone.

As an alternative, β-titanium (β-Ti) alloys were investigated (Farrahnoor and Zuhailawati, 2021; Johannsen et al., 2023; Niinomi, 1998) which are providing a lower Young's modulus (higher elasticity) compared to Ti–6Al–4V, Co–28Cr–6Mo alloy and oxide ceramics (Niinomi, 1998), thus potentially reducing the stress shielding. The elasticity and excellent biocompatibility are traced back to the body-centered cubic crystal structure stabilized by biocompatible elements such as niobium, tantalum, and zirconium (Eisenbarth et al., 2004; Farrahnoor and Zuhailawati, 2021; Niinomi, 1998). In addition to their suitable properties, certain β-Ti alloys, e.g. Ti–Nb (Pilz et al., 2022; Schulze et al., 2018), Ti–Nb–Ta (Johannsen et al., 2023; Sass et al., 2024c), and Ti–Nb–Ta–Zr (Luo et al., 2019; Ozan et al., 2017) can be additively manufactured, which is advantageous in terms of design freedom and fabrication of open porous surface structures, e.g. flexible surface designs (Sass et al., 2023), for enhanced implant-bone interaction (Ni et al., 2019; Song et al., 2023). However, titanium and its alloys have a lower wear resistance and, therefore, cannot be applied for high tribologically stressed implant parts (Kaur and Singh, 2019).

To address clinical issues with CoCrMo-based femoral components, PEEK (Post et al., 2022; Ruiter et al., 2017, 2021), multifunctional materials (Bahraminasab et al., 2017, 2019, 2021, 2022a, 2022b; Mick et al., 2015; Sass et al., 2024a; Sun et al., 2022) or wear-resistant coatings on titanium-based implants (Galas et al., 2023; Lee et al., 2023) have been investigated. In this regard, multifunctional materials are defined by the combination of a ceramic-based implant component in the articulating contact zone and a titanium-based implant component in the bone interface to meet the diverse requirements of an advanced implant material for TKR (Bahraminasab et al., 2017, 2019, 2021, 2022a, 2022b; Mick et al., 2015; Sass et al., 2024a; Sun et al., 2022). These materials may combine the advantageous properties by reducing the specific limitations of each monolithic material. Functionally graded materials with an increasing Ti–6Al–4V content from the pure oxide ceramic component to the bone interface, produced by spark laser sintering, have been investigated (Bahraminasab et al., 2017, 2019, 2021, 2022a, 2022b; Moayedee et al., 2024). Soldering ceramic and titanium components with a glass solder to create a hybrid material is another conceivable approach. Joining dissimilar materials is challenging but can be achieved (Mick et al., 2015; Sass et al., 2024a; Suansuwan and Swain, 2003; Sun et al., 2022; Vásquez et al., 2009). During a firing process, a material bond is formed by diffusion of elements and the formation of interlayers (Mick et al., 2015; Sass et al., 2024a; Sun et al., 2022; Vásquez et al., 2009) and mechanical interlocking (Sun et al., 2022). Despite promising results of joined orthopedic materials (Ti–6Al–4V/ATZ (Mick et al., 2015), Ti–35Nb–6Ta/ATZ (Sass et al., 2024a)), the concept of a hybrid material-based femoral component for TKR using glass soldering of subcomponents has not been studied.

Furthermore, previous studies investigating alternative implant materials for the femoral component of a TKR have been focused on the bone-implant interaction (Bahraminasab et al., 2013; Galas et al., 2023; Ruiter et al., 2021) to prove the reduced stress shielding but the mechanical loading of the femoral component induced during the implantation procedure has not been considered. Since Kluess et al. (2012) clearly described the risk of intraoperative fracture of ceramic femoral components caused by anterior-posterior opening ("wedge load"), it is essential to investigate the influence of the hybrid material in this loading scenario as well.

Hence, the present study aimed to analyze the biomechanical properties of a hybrid material-based femoral component for TKR using finite element (FE) modeling. For this purpose, the hybrid material was realized by bonding ATZ ceramics to Ti–6Al–4V or Ti–35Nb–6Ta alloys. We investigated the stresses and strains within the femoral component and the periprosthetic bone under mechanical loading induced by the uncemented implantation and during a two-legged squat motion up to ~90° knee flexion. The squat motion was based on a numerical workflow, where a musculoskeletal multibody simulation (MMBS) of the lower extremity was sequentially linked to the FE model.

2. Materials and methods

2.1. Study overview

This study investigated the influence of the femoral component material on the biomechanical properties using a right cruciate-retaining TKR (Columbus®, Aesculap AG, Tuttlingen, Germany). The tibial insert and resurfaced patellar component were considered within the two-legged squat motion. Four different materials were defined for the femoral component: hybrid materials of ATZ and Ti–6Al–4V (Ti–6Al–4V/ATZ) or ATZ and Ti–35Nb–6Ta (Ti–35Nb–6Ta/ATZ), monolithic Co–28Cr–6Mo alloy, and monolithic ATZ ceramic. The Ti–35Nb–6Ta/ATZ hybrid material has been recently experimentally characterized and showed promising mechanical and biological properties (Sass et al., 2024a). The additively manufactured titanium components were completely dense or had an open porous surface structure. Implant loading during uncemented implantation and stress shielding within the periprosthetic bone during two-legged squat motion was evaluated by comparing the strain energy density in defined regions of interest (ROI). Most of the model input parameters were taken from the literature. Since no data were available on the elastic properties of open porous Ti–35Nb–6Ta lattice structures for the functionalized implant surface, mechanical tests of material specimens were carried out accordingly.

2.2. Experimental characterization of open porous lattice structures

2.2.1. Specimen preparation

For detailed information on the preparation of the pre-alloyed Ti–35Nb–6Ta powders and the process parameters, we refer to a previous study by Johannsen et al. (2023). In brief, the Ti–35Nb–6Ta specimens were produced by laser beam powder bed fusion (PBF-LB/M) using a DMP350 Flex (3D Systems Corp., Rock Hill, SC, USA) equipped with a 1 kW single-mode laser (YLR-1000-WC-Y14, IPG Laser GmbH, Burbach, Germany). Ti–6Al–4V specimens were prepared using a SLM500 Quad (SLM Solutions Group AG, Luebeck, Germany) (Sass et al., 2024c). The defined process led to chemical homogenous Ti–35Nb–6Ta specimens having a pure β crystal structure and densities >99 % (Johannsen et al., 2023). Open porous lattice structures were designed with a $1 \times 1 \times 1$ mm^3 face-centered cubic unit cell in Creo Parametrics 6.0.3.0 (PTC Inc., Boston, MA, USA) based on a previous study (Sass et al., 2024c). The strut diameter and resulting nominal porosity were 0.3 mm and 70 %, respectively. Rectangular specimens measuring $7 \times 7 \times 11$ mm^3 were prepared for experimental compression tests (Fig. 1A).

2.2.2. Mechanical characterization

The open porous specimens ($n = 5$) were axially loaded to failure using a universal testing machine (Z050-50 kN, Zwick Roell, Ulm, Germany) at a crosshead speed of 0.005 mm × s^{-1} (Sass et al., 2024c). The stress-strain curves were obtained using a tactile extensometer (digiClip Extensometer, Zwick Roell, Ulm, Germany), and the compressive modulus (C), the compressive yield strength ($\sigma_{C,0.2}$) the ultimate compressive strength (UCS), and the elongation at break (ε) were evaluated. The test setup is shown in Fig. 1B.

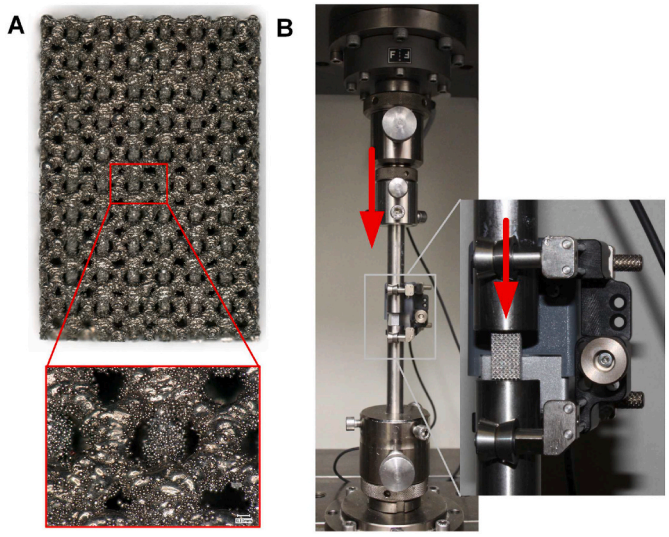

Fig. 1. A) Rectangular open porous specimen for axial compression test with a detailed view of the lattice structure and B) setup for mechanical testing indicating the compression force vector.

2.2.3. Statistical analysis

Statistical analysis of the experimental data was performed in SPSS statistics (v25, IBM Corp., Armonk, NY, USA), and the level of significance was $p < 0.05$ for all tests. All groups were tested for statistical significance using an independent *t*-test after evaluating its applicability regarding the groups' normal distribution and variance homogeneity.

2.3. Finite-element simulation

2.3.1. General model assumptions, material properties, and discretization strategy

Two quasi-static FE models were developed in Abaqus v2022 (Dassault Systèmes, Providence, RI, USA) using the implicit solver resembling the uncemented implantation and the two-legged squat motion. For both models, the CT scan of a human femur (male, 83 years old, body weight of 61 kg) was reconstructed using Mimics 25.0 (Materialise NV, Leuven, Belgium) and sectioned 10 mm above the femoral component. Virtual implantation of the femoral component was performed according to the surgical guidelines and was reviewed by an experienced orthopedic surgeon.

The established implant design was modified to create a biphasic design (Fig. 2) with fully constrained interfaces between the subcomponents. This artificial design was used to study the hybrid material-based femoral components. The titanium component had a constant thickness of 3 mm (excluding the two pins). In addition, models with an open porous surface (1 mm thick) have been designed, which may enhance bone-implant interaction (Galas et al., 2023; Gao et al., 2019). Accordingly, the material interface was always defined by dense material components.

The modeled material properties are summarized in Table 1. All materials were assumed to have isotropic and linear elastic material properties. Heterogeneous bone properties were based on the correlation between Young's modulus and Hounsfield units (HU) for the cortical (ash density $\geq 0.6\ g \times cm^{-3}$) and trabecular (ash density $<0.6\ g \times cm^{-3}$) bone (Keyak and Falkinstein, 2003) of the distal femur in the superior-inferior direction (Rho et al., 1995). The correlation functions were chosen as they directly refer to bone specimens extracted from human distal femurs. A phantom-based calibration (QRM, Moehrendorf, Germany) was performed to define the correlation between apparent density and HU, and further, the apparent density was transformed into ash density (Schileo et al., 2008). In Abaqus v2022, a node-based assignment of Young's moduli was performed using a self-written plug-in (Mauck et al., 2016). Each node obtains an HU value derived from the CT data using the corresponding node coordinates. The HU values are considered as virtual temperatures to simulate the heterogeneous bone material properties in vivo by a linear-elastic temperature-dependent material model. The frequency of assigned Young's moduli, the curve of the Young's moduli as a function of the HU, and the assigned corresponding Young's moduli are shown in Fig. 3.

Femoral component materials (hybrid materials, Co–28Cr–6Mo alloy, ATZ ceramic) and UHMW-PE for the tibial insert and patellar component were assumed to be homogeneous. The open porous surface structure of the titanium part of the femoral component was represented by the experimentally determined compressive stiffness and not by modeling the actual geometry of the lattice structures. In addition to the elastic properties, UHMW-PE was modeled with a plastic material

Table 1
Defined material properties for finite element modeling (E_{Cort}: Young's modulus of the cortical bone, E_{Trab}: Young's modulus of the trabecular bone, ρ: ash density).

Material	Young's modulus [GPa]	Poisson's ratio	Reference
Bone	$E_{Cort} = -6.142 \times 0.014 \times \rho$ $E_{Trab} = 0.82 \times \rho^{1.27}$	0.4	Rho et al. (1995)
Co–28Cr–6Mo	240	0.3	Galas et al. (2023)
UHMW-PE	0.239	0.35	Sauer et al. (2021)
ATZ	261	0.27	Vogel et al. (2021)
Ti–6Al–4V	110	0.3	Niinomi (1998)
Open porous Ti–6Al–4V	8.8	0.3	Current study
Ti–35Nb–6Ta[a]	63	0.3	Sass et al. (2024c)
Open porous Ti–35Nb–6Ta	5.2	0.3	Current study

[a] Averaged compressive modulus of specimens manufactured in three different build directions during laser beam powder bed fusion.

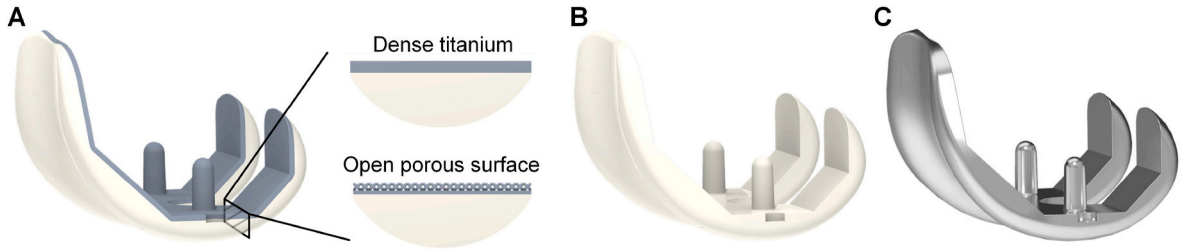

Fig. 2. Geometries of the analyzed femoral components of a total knee replacement (figures created in Creo Parametrics 6.0.3.0) made of A) a hybrid material of ATZ ceramic (articulating surface) and a titanium alloy (bone interacting surface), and section views of the hybrid material-based femoral component showing the titanium-based component with/without an open porous surface structure, B) monolithic ATZ ceramic and C) monolithic Co–28Cr–6Mo alloy.

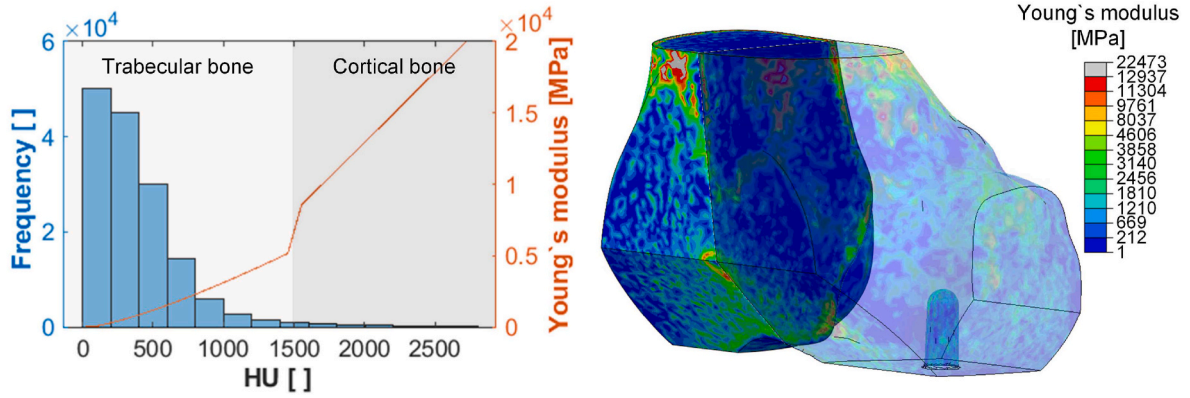

Fig. 3. Frequency and Young's moduli as a function of the Hounsfield unit (HU) according to Rho et al. (1995) of the distal femur used for the finite element analysis and the assigned heterogenous Young's moduli in Abaqus v2022 that corresponds to the HU.

behavior (yield strength: 25 MPa) (Sauer et al., 2021).

Quadratic tetrahedron elements (C3D10) were used to discretize the model. The element sizes were defined within a convergence analysis where the number of elements was incrementally increased. The maximum stress in the femoral component during uncemented implantation and the strain energy in the femoral bone during two-legged squat motion were evaluated. Convergence was defined as a change in the outcome measures of less than 5% compared to the next finer mesh. The defined element edge lengths of the model representing uncemented implantation were 1.4 mm for the ATZ component. The dense and open porous titanium components were meshed with an element edge length of 0.6 mm and 1.1 mm, respectively. The regions of maximum stress in the titanium components were finer meshed with an element edge length of 0.3 mm and a minimum of four elements across the thickness. In the squatting model, element edge lengths of 2.2 mm, 1.5 mm, and 2.2 mm were used for the ATZ component, the titanium components, and the femoral bone, respectively. In addition, the tibial insert and the patellar component were meshed with element edge lengths of 3 mm. Further details of the mesh and convergence study can be found in the Supplementary Material.

2.3.2. Boundary conditions and interaction properties during implantation

The assembly and the boundary conditions of the uncemented implantation are shown in Fig. 4A. Based on literature studies (Berahmani et al., 2017; Post et al., 2022), an interference fit of 1 mm was created between bone and implant in the anterior-posterior direction. We did not model the implantation by forcing the implant onto the bone, but instead used the remove interference fit option in the contact module. In this step, the surface nodes of the bone (secondary surface) are moved incrementally toward the implant surface (main surface) (Berahmani et al., 2017). In addition, the implant was moved 0.5 mm distally to remove the superior-inferior interference fit. This translational constraint was applied to a coupled reference point (F_{RP}). The bone was fixed proximally throughout the simulation by fully constraining a coupled reference point (B_{RP}). The implantation results in maximum stresses in the lateral posterior radius, as shown in Fig. 4B.

The bone-implant contact was modeled as a hard surface-to-surface contact and with a frictionless penalty contact. Since the friction of the interface did not affect the results with the defined boundary conditions, we simplified the model with this assumption and reduced the run time and convergence errors caused by frictional contact.

2.3.3. Boundary and contact conditions of the two-legged squat motion

The model assembly and the boundary conditions of the two-legged squat motion are shown in Fig. 5. The boundary conditions were derived from a previously described MMBS (Kebbach et al., 2020, 2023; Tischer et al., 2023) and are shown in Fig. 5A. The squat motion was chosen because it covers a wide range of motion and has been previously used to

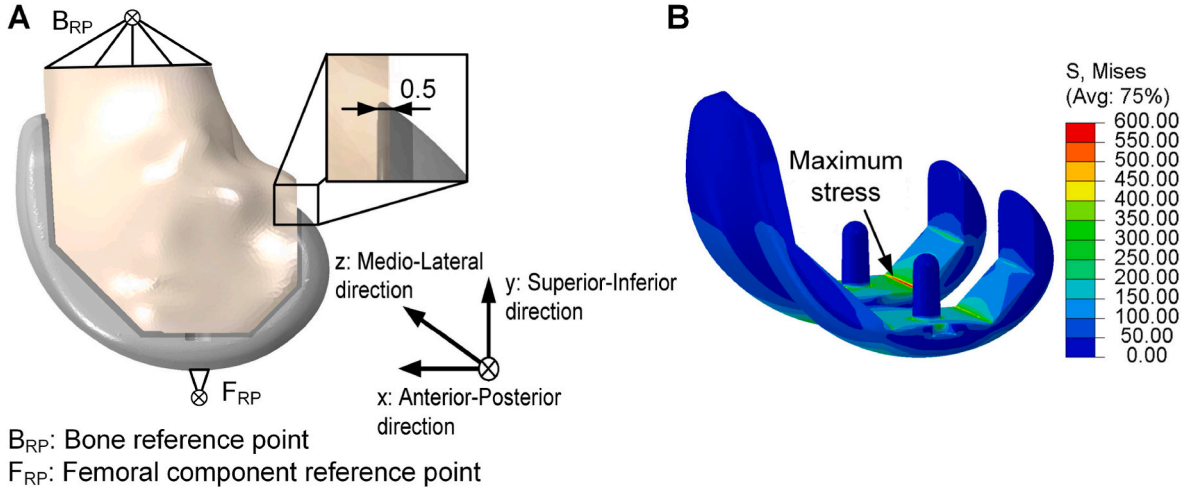

Fig. 4. Finite element model of the uncemented implantation of the femoral component: A) model assembly with initial position of the femoral component and femoral bone (total interference fit in anterior-posterior direction of 1 mm) and identification of the reference points (B_{RP}: fully constrained during loading, F_{RP}: displaced in superior-inferior direction for implantation, free translation in x-direction and constrained in z-direction and all rotational degrees of freedom) and B) location of the maximum von Mises stresses (in MPa) during the implantation.

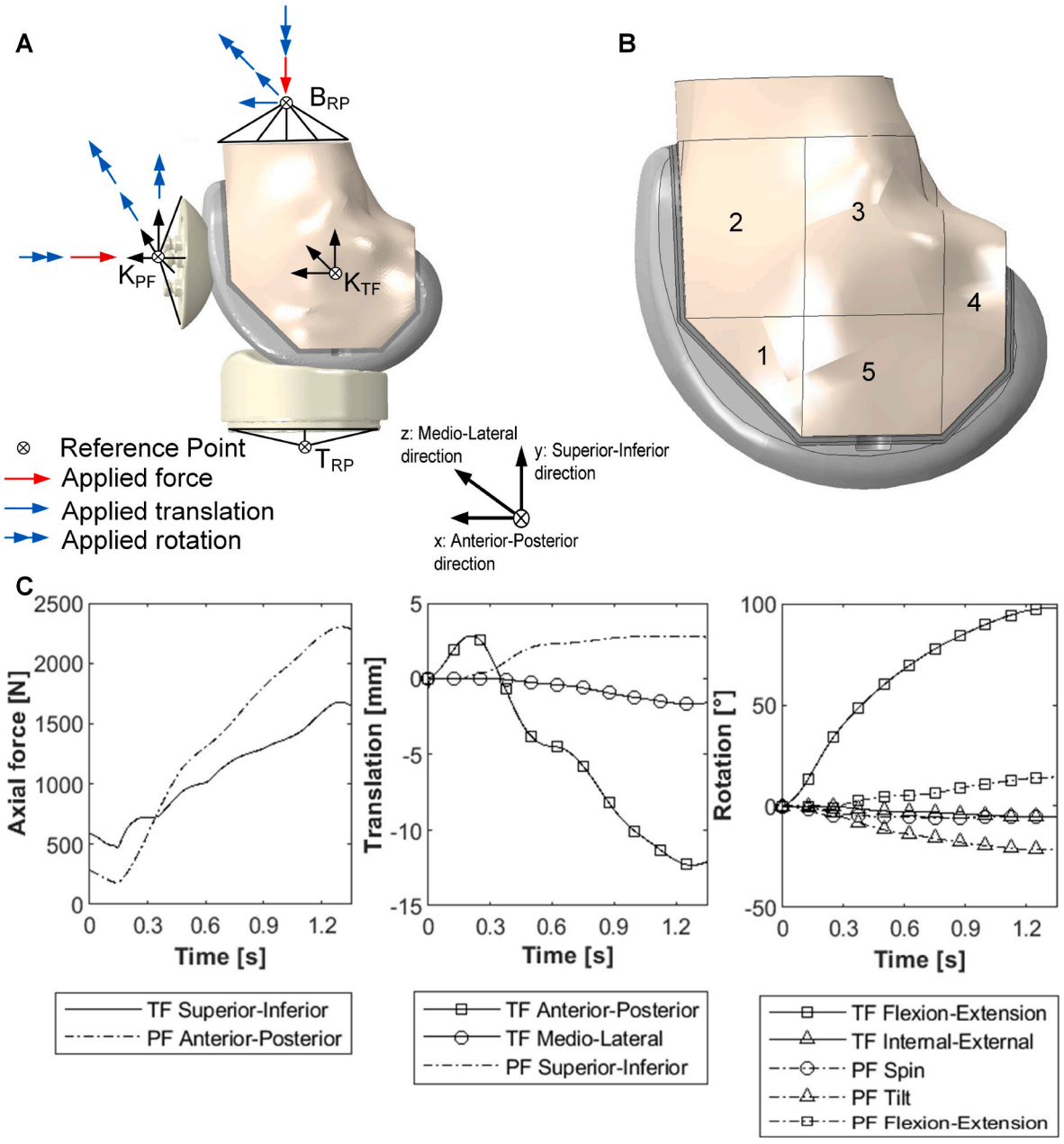

Fig. 5. Finite element model of the two-legged squat motion to ~90° of knee flexion: A) initial position of the femoral component, tibial insert and patellar component, where the defined local coordinate systems for the tibiofemoral (K_{TF}) and patellofemoral joint (K_{PF}), the reference points (B_{RP}, T_{RP}) and the applied boundary conditions derived from the musculoskeletal multibody simulation are indicated, B) defined regions of interest 1 to 5 to analyze the volumetric stress shielding by the strain energy density as a function of knee flexion angle and femoral component material, and C) tibiofemoral (TF) and patellofemoral (PF) joint forces, translations and rotations applied to the reference points.

study bone-implant load transfer in TKR (Ruiter et al., 2017; van Jonbergen et al., 2012). The FE model contains the tibial insert, the resurfaced patellar component, the femoral component, and the distal femur. The methodology to link the MMBS and FE analysis followed the workflow according to our previous work (Sass et al., 2024b).

The MMBS was based on the dataset of the 4th Grand Knee Challenge Competition (Fregly et al., 2012) and was built in SIMPACK V9.7 (Dassault Systèmes, Providence, RI, USA). The model used a non-linear force-strain relationship for relevant ligaments of the tibiofemoral and patellofemoral joint, and the articulating implant surfaces were constrained using a polygonal contact model. To calculate the muscle forces, joint coordinates from motion capturing were used in a forward dynamic MMBS using a computed muscle controller with static optimization and wrapping algorithm (Kebbach et al., 2020). Concerning the implant design, the previous implant components were replaced with those described in section 2.1. The kinematics and contact forces of the tibiofemoral and patellofemoral joints (Fig. 5c) were calculated in the MMBS and then transferred to fixed local coordinate systems in Abaqus v2022 (tibiofemoral K_{TF}, patellofemoral K_{PF}, see Fig. 5A). The joint kinematics were further transferred to the bone reference point (B_{RP}), which was kinematically coupled to the distal cut surface of the femur. Five bone ROI (see Fig. 5B) were defined in the distal femur (Meneghini et al., 2015; Ruiter et al., 2021) to assess the influence of the implant material on volumetric stress shielding.

During the two-legged squat motion, the implant was assumed to be osseointegrated, which was modeled with a fully constrained interface (tie constraint) between the femoral component (main surface) and bone (secondary surface). In addition, ATZ ceramic or Co–28Cr–6Mo alloy

articulating surfaces in contact with UHMW-PE were modeled as hard surface-to-surface contact with a coefficient of friction of 0.04 (Godest et al., 2002).

2.3.4. Outcome measures

The maximum stress in the femoral component was evaluated during the uncemented implantation. This was performed separately for each model component in the hybrid material-based femoral components. Due to the different intrinsic material properties (brittle vs. ductile), the maximum principal stress was used for the ATZ ceramic, and the maximum von Mises stress was used for the Co–28Cr–6Mo alloy and the titanium alloys. During squatting, the relative change in strain energy density compared to the ATZ femoral component in the defined bone ROI was evaluated for each time step. The strain energy density has been described as a stimulus for bone remodeling (Carter et al., 1987; Huiskes et al., 1987) and has previously been used to study the influence of the implant material on volumetric stress shielding around the femoral component (Ruiter et al., 2021). The increase in the strain energy density compared to the defined reference indicates an improvement in the load transfer from the implant to the adjacent bone as the bone is subjected to higher strains.

3. Results

3.1. Mechanical characterization

Representative stress-strain curves of the open porous lattice structures are shown in Fig. 6. Specimens of both titanium alloys fractured at ~45° to the load axis, with Ti–35Nb–6Ta exhibiting extensive ductile behavior.

The determined mechanical properties and their level of significance are shown in Table 2. The Ti–35Nb–6Ta specimens showed a higher elasticity, ultimate compressive strength, and elongation at break but decreased yield strength compared to the Ti–6Al–4V specimens.

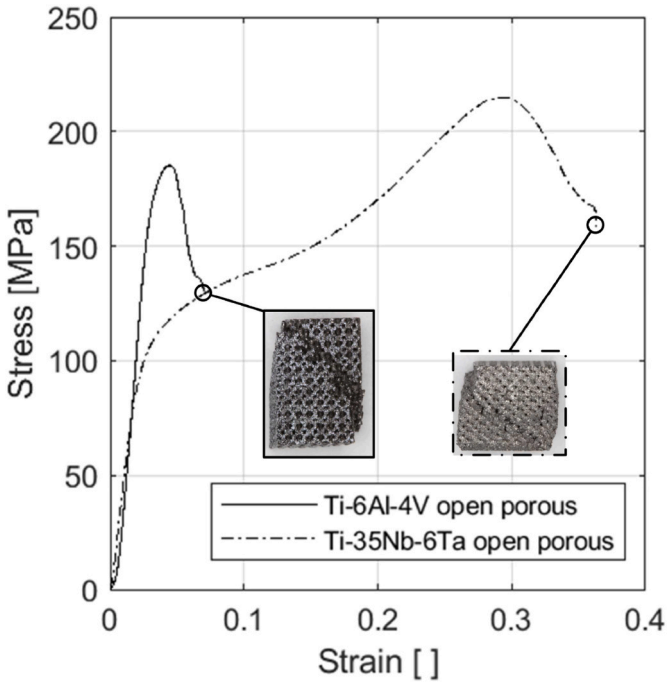

Fig. 6. Representative stress-strain curves of rectangular (7 × 7 × 11 mm^3) open porous structured specimens made of Ti–6Al–4V or Ti–35Nb–6Ta and illustration of the macroscopic fracture.

3.2. Finite-element simulation of the implantation

The maximum stress during implantation was observed in the lateral, posterior radius of the uncemented femoral components and at the final position of the implantation since the anterior-posterior opening was the largest there. Fig. 7 compares the different stress distributions of the hybrid material-based femoral component made of Ti–35Nb–6Ta/ATZ with and without an open porous surface structure of the titanium part and of the monolithic ATZ femoral component.

The maximum principal stress in the monolithic ATZ femoral component amounted to 1568.9 MPa, and the maximum von Mises stress in the Co–28Cr–6Mo based femoral component was 1290.6 MPa. The maximum principal stress in the ATZ component decreased within the hybrid material-based femoral components to 367.6 MPa (−76.6 %) for Ti–6Al–4V/ATZ, to 560.9 MPa (−64.3 %) for Ti–6Al–4V/ATZ with an open porous surface structure, to 474.9 MPa (−69.7 %) for Ti–35Nb–6Ta/ATZ, and to 648.4 MPa (−58.7 %) for Ti–35Nb–6Ta/ATZ with an open porous surface structure. The maximum von Mises stresses in the titanium-based implant parts were 758.2 MPa (Ti–6Al–4V/ATZ), 636.5 MPa (Ti–6Al–4V/ATZ with an open porous surface structure), 506.2 MPa (Ti–35Nb–6Ta/ATZ), and 411.1 MPa (Ti–35Nb–6Ta/ATZ with an open porous surface structure). The maximum von Mises stress in the open porous surface layer was 52.6 MPa and 84.2 MPa in the Ti–35Nb–6Ta and Ti–6Al–4V implant components, respectively.

Accordingly, we observed that the stress within the ATZ part of a hybrid material-based femoral component is influenced by Young's modulus and the structural stiffness of the joined titanium part.

3.3. Finite element simulation of the squat motion

The strain energy density in the anterior region of the distal femur (ROI 1) as a function of the knee flexion angle is shown in Fig. 8 as a representative curve of the analyzed models during the two-legged squat motion. It can be seen that the strain energy density increased at higher flexion angles due to a higher axial joint force. In addition, the hybrid materials increased the strain energy density and, therefore, the load on the bone. The effect of the different implant materials is clearly pronounced in bone ROI 1 at approximately 35° of knee flexion. The strain energy density of the periprosthetic bone was influenced by both the titanium alloy used and the implant surface structure (dense or open porous).

The relative changes in strain energy density (ΔSED) within the bone ROIs of the different femoral component materials compared to monolithic ATZ ceramic are shown in Fig. 9. We observed minor differences between ATZ ceramic and Co–28Cr–6Mo alloy, based on their comparable Young's moduli (ATZ: 261 GPa vs. Co–28Cr–6Mo: 240 GPa). The hybrid materials distinctively increased the strain energy density in the anterior region of the periprosthetic bone (ROI 1 and 5). For example in the bone ROI 1 at ~90° of knee flexion, the strain energy density increased by 25.7% (Ti–6Al–4V/ATZ), 70.3% (Ti–6Al–4V/ATZ with an open porous surface), 43.7% (Ti–35Nb–6Ta/ATZ), 82.5% (Ti–35Nb–6Ta/ATZ with an open porous surface), and 4.8% (Co–28Cr–6Mo alloy) compared to monolithic ATZ.

4. Discussion

To avoid metal ion release, stress shielding, and subsequent aseptic implant loosening, current advances in implant materials for femoral components of TKR represent polymers such as PEEK (Post et al., 2022; Ruiter et al., 2017, 2021), functionally graded materials (Bahraminasab et al., 2017, 2021, 2022a, 2022b; Moayedee et al., 2024), or wear-resistant coatings on titanium-based implants (Galas et al., 2023; Lee et al., 2023). In line with these approaches, soldering of ceramic and titanium subcomponents to form a hybrid material is a promising approach in TKR that has been investigated in a recent experimental study of our group (Sass et al., 2024a). However, this study was limited

Table 2
Mechanical properties of the compressively loaded open porous lattice structures and the level of significance between Ti–35Nb–6Ta and Ti–6Al–4V specimens. C: compressive modulus, $\sigma_{C,0.2}$: compressive yield strength, UCS: compressive ultimate strength, ε: elongation at break.

	C [GPa]		$\sigma_{C,0.2}$ [MPa]		UCS [MPa]		ε [ ]	
Ti–35Nb–6Ta	5.2	(0.2)	89.9	(0.6)	226.5	(32.2)	0.35	(0.03)
Ti–6Al–4V	8.8	(0.8)	163.1	(2.6)	183.7	(2.4)	0.12	(0.02)
p-value	<0.001		<0.001		0.029		<0.001	

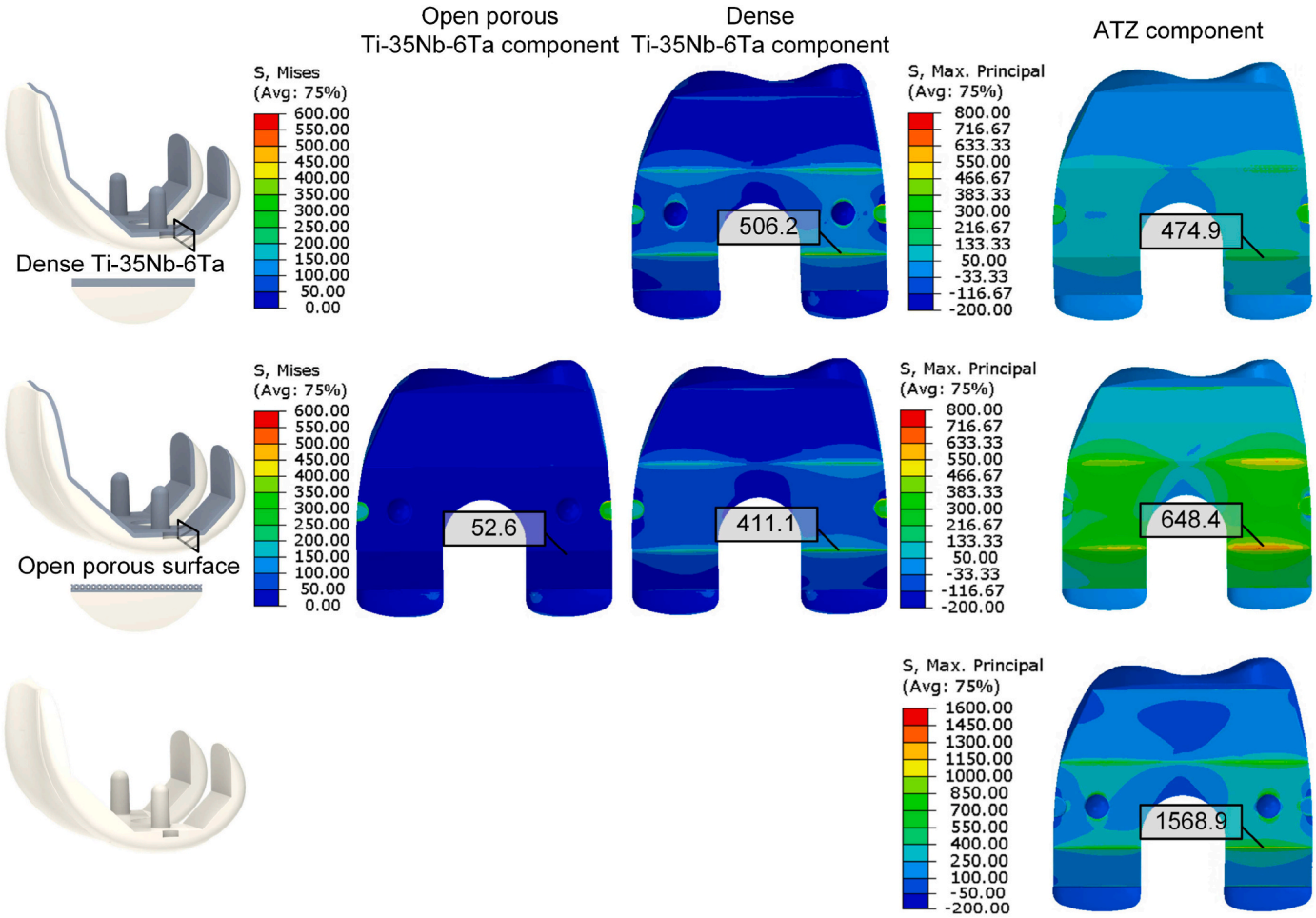

Fig. 7. Stress distributions (von Mises or maximum principal stress, both in MPa) of the finite element models simulating implantation of uncemented femoral components consisting of Ti–35Nb–6Ta/ATZ hybrid materials with/without an open porous surface structure, and monolithic ATZ.

by simplified geometries, and the performance during implantation and the bone-implant interactions have not been investigated so far. Hence, we used the FE analysis to evaluate the biomechanical properties of a hybrid material-based femoral component based on an oxide ceramic component in the articulating interfaces and a titanium-based component in the bone-implant interface. The titanium alloys were Ti–6Al–4V or Ti–35Nb–6Ta (pure β-Ti), which were modeled either completely dense or with an open porous surface structure. We analyzed implant loading scenarios by uncemented implantation and bone-implant interaction during two-legged squat motion.

Uncemented implantation of the femoral component has benefits compared to cemented fixation (Uivaraseanu et al., 2022) but is a high-impact event and results in an anterior-posterior opening of the femoral component, comparable to the loading of cemented implantation with distal under resection of the femur (Kluess et al., 2012). Several studies have experimentally and numerically investigated the implantation of femoral components (Berahmani et al., 2015, 2017; Kluess et al., 2010, 2012). During implantation, higher stresses in ceramic-based femoral component compared with a femoral component made of Co–28Cr–6Mo alloy were observed and critical maximum principal stresses of up to ~2000 MPa were reported in the radius of the transition from the distal horizontal section to the anterior and posterior oblique sections (Kluess et al., 2010, 2012). In our present study, a maximum principal stress of 1568.9 MPa has been demonstrated in the monolithic ATZ-based femoral component, which was comparable to these previous observations. Although ATZ ceramics have a relatively high fracture toughness compared to other ceramics (Bedir et al., 2023), it is characterized by brittle fracture (Roulet et al., 2021; Sequeira et al., 2017), and studies reported maximum flexural strength of 1394 MPa (Sequeira et al., 2017) and maximum biaxial strength of 1636 ± 302 MPa (Roulet et al., 2021). Therefore, the maximum principal stress in the monolithic ATZ femoral component in this study was within a critical range of material failure, indicating the risk of intraoperative fracture. The observed stress in the titanium components was below the yield strength of the materials (Sass et al., 2024c), and the stress in the open porous surface layer also did not exceed the yield strength. Thus,

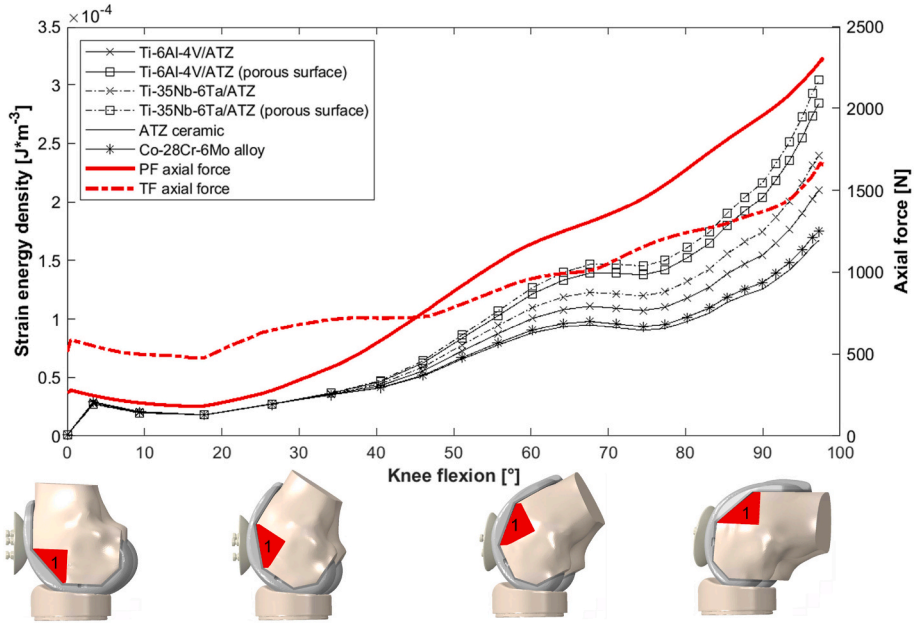

Fig. 8. Strain energy density in the bone region of interest one as a function of the knee flexion angle and the axial force distribution at the tibiofemoral (TF) and patellofemoral (PF) joints and comparison of the different femoral component materials (hybrid materials of Ti–6Al–4V/ATZ and Ti–35Nb–6Ta/ATZ with and without an open porous surface structure, monolithic ATZ ceramic and monolithic Co–28Cr–6Mo alloy).

the mechanical integrity of the titanium components was maintained during cementless implantation.

We found a distinctive stress reduction in the ATZ component within the hybrid material-based implants ranging from −76.6 % to −58.7 %, depending on the model configuration. Our observations showed that in the hybrid material concept, the titanium component shields the ATZ component from high stresses. This phenomenon depends on the area moment of inertia of the implant components. Accordingly, when the elasticity of the titanium alloy increases, the stress in the ATZ component increases as well, while the stress in the titanium component decreases. The design optimization of the components is crucial for sufficient implant safety during uncemented implantation since the area moment of inertia is determined by the intrinsic material properties and the geometrical property (e.g. wall thickness).

Stress shielding of the periprosthetic bone is caused by the altered load transfer to the distal femoral bone after TKR. Implant materials with a higher stiffness than bone led to a biomechanical situation in which forces are carried predominantly by the implant components and not by the bone. According to Wolff's law (Wolff, 2010), the altered bone loading induces stress-related bone resorption (Galas et al., 2023; Ruiter et al., 2021). We found that there were no differences between ATZ ceramic and Co–28Cr–6Mo alloy based femoral components in terms of stress shielding. This is reasonable because ATZ and Co–28Cr–6Mo have almost similar Young's moduli. Due to the higher elasticity of the titanium alloys, the hybrid femoral components reduced the stress shielding of the periprosthetic bone compared to monolithic ATZ and Co–28Cr–6Mo. Previous studies have investigated the effect of the implant material on the stress shielding (Bahraminasab et al., 2013; Galas et al., 2023; Ruiter et al., 2021) and confirm our current observations. A comparison of PEEK (Ruiter et al., 2021), Ti–6Al–4V with Ti–Nb–N coating (Galas et al., 2023), or a functionally graded material (Bahraminasab et al., 2013) indicated that stress shielding decreases with higher elasticity of the implant materials. Our results highlight the beneficial effects of β-Ti alloys such as Ti–35Nb–6Ta and the design of open porous implant surface structures to reduce the stress shielding within the periprosthetic bone. The applied lattice structures used for experimental characterization were only one example of various design possibilities. Despite achieving compressive stiffness in the range of human bone, further optimization, or other designs should be considered.

Clinical studies have analyzed bone resorption after TKR with radiographic measurements of bone density (Bendich et al., 2022; Järvenpää et al., 2014; Lee et al., 2023; Mintzer et al., 1990; Yilmaz et al., 2021). These studies have demonstrated that the anterior part of the distal femoral bone is particularly affected. This region is comparable to our described bone ROI 1 and 5. The hybrid femoral components showed the highest improvement in implant-to-bone load transfer in this region, indicating potential to reduce clinically relevant bone resorption. In this context, a comparison of different implant materials has not been performed in clinical studies so far.

This computational study has limitations. The FE analysis was based on one femoral component design implanted in one femur. Therefore, anatomical variations or different bone conditions were not considered. For uncemented implantation, only one press-fit was considered, and the linear-elastic material assumptions of the bone may overestimate the implant load because the bone is plastically deformed during uncemented implantation (Berahmani et al., 2017). Cementless implanted ATZ ceramic or Co–28Cr–6Mo alloy-based femoral components necessarily require surface functionalization, e.g. titanium plasma spray coating, to achieve osseointegration, which was neglected in the simulations of this present study. Furthermore, the dynamic impaction during implantation was simplified to a static model, but we based our modeling on a previous study (Berahmani et al., 2017). In addition, the derived boundary conditions of the two-legged squat motion were based on a MMBS of the lower extremity, with its limitations described in detail by Kebbach et al. (2020). In addition, no experimental study has been conducted to manufacture a hybrid material-based femoral component so far. Hence, because the numerical simulations have not been experimentally validated, the absolute results have to be interpreted with restrictions. However, general observations of the simulations are consistent with other previously published studies. Accordingly, this computational study should be considered as a systematic comparison of the different implant materials and as a first evaluation rather than as a determination of absolute values. Moreover, glass soldering is a viable technology for bonding ATZ ceramics to titanium materials, creating a material bond and mechanical interlock

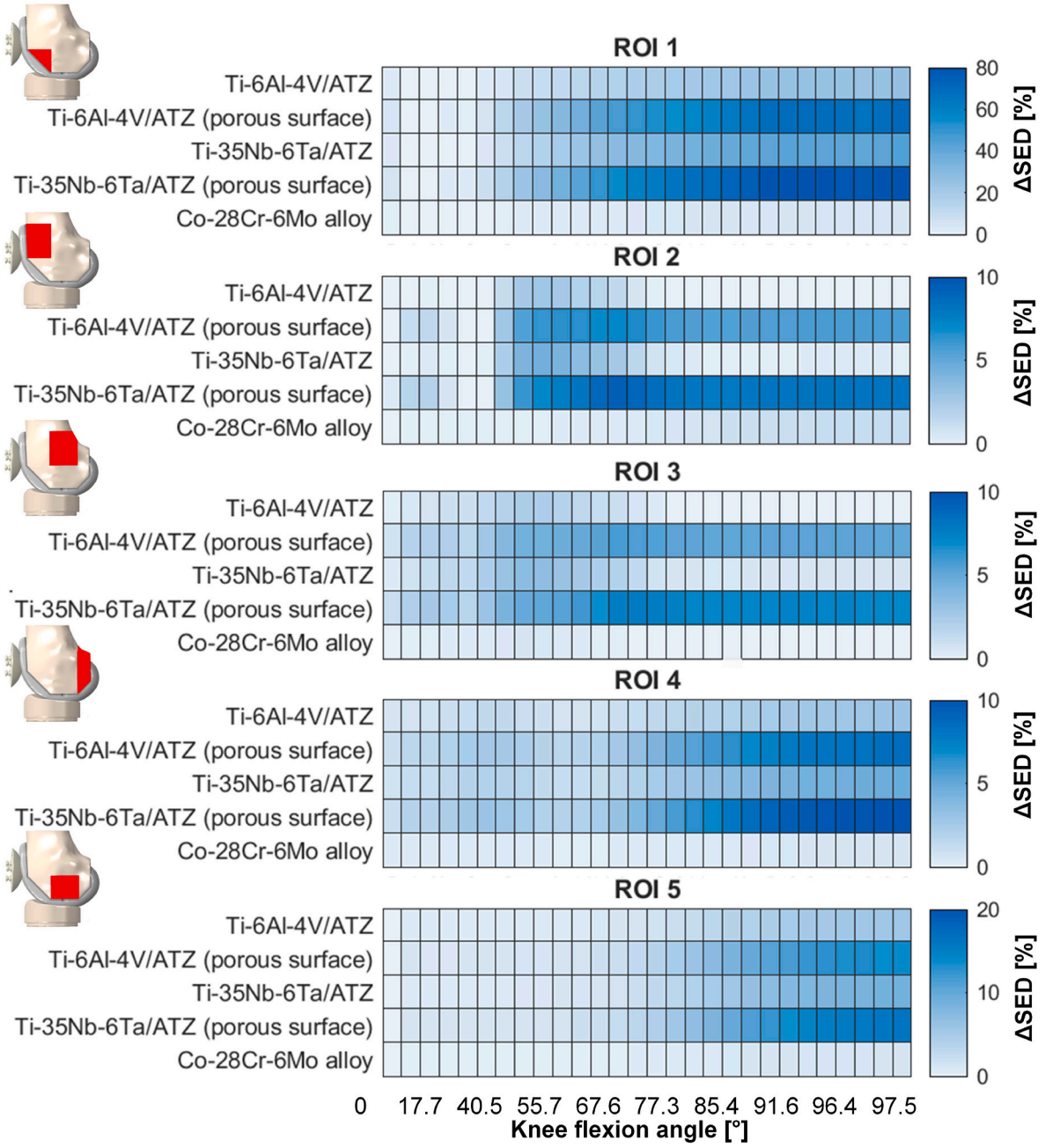

Fig. 9. Heat maps of the relative change in strain energy density (ΔSED [%]) for the different bone regions of interest (ROI) compared to the ATZ ceramic-based femoral component as a function of the implant material (hybrid materials of Ti–6Al–4V/ATZ and Ti–35Nb–6Ta/ATZ with dense or an open porous surface structure, and monolithic Co–28Cr–6Mo alloy).

during firing (Mick et al., 2015; Sass et al., 2024a; Suansuwan and Swain, 2003; Sun et al., 2022; Vásquez et al., 2009). In our present study, the soldered joint was considered only by constrained interfaces and not by volumetric modeling of the glass solder. However, the investigation of the interface stresses and the joint strength of the material bond are of great importance, since failure is likely to occur within the glass-solder or the titanium alloy surface (Sass et al., 2024a). In our previous study on the experimental characterization of TiNbTa/ATZ specimens, we concluded that a diffusion layer is formed at the glass-solder/TiNbTa interface (Sass et al., 2024a), and it is reasonable to assume that this has different material properties than the bulk TiNbTa alloy. Furthermore, thin joints (~0.1 mm (Sass et al., 2024a)) pose challenges in FE modeling, which could be solved by sub-modeling of certain locations.

The transfer of the glass soldering technology to Ti–35Nb–6Ta and the development of a functional demonstrator are part of subsequent studies. Future studies should focus on various aspects, including the press fit required to achieve primary stability, the influence of design specifications, and patient-specific factors such as bone quality and individual motion sequences. Assuming a glass-soldered bond between the materials, it is crucial to develop a reliable FE model of the material joint and to comprehensively analyze the factors influencing the joint strength. In addition, worst-case scenarios such as under-resection during implantation or dynamic impactions induced by falls or accidents could be considered to further evaluate the performance of hybrid implant materials.

5. Conclusion

The purpose of this computational study was to analyze hybrid materials for the uncemented femoral component by evaluating their biomechanical properties during implantation and two-legged squat motion. The hybrid material was based on ATZ ceramics for the articulating surface and different titanium alloys (Ti–6Al–4V or Ti–35Nb–6Ta) for the bone-implant interface. In the FE modeling, the hybrid femoral component showed a reduced fracture risk within the ceramic part compared to the monolithic ceramic implant for the investigated uncemented implantation. In addition, the stress shielding in the periprosthetic bone is mainly reduced in the anterior region, where bone resorption has been primarily observed in clinical studies. The combination of ATZ ceramics and titanium alloys in a multifunctional material potentially combines the high wear and corrosion resistance of ATZ ceramics with the osseoconductivity and high elasticity of the TiNbTa alloy. At the same time, limitations such as brittle fracture of the ceramic and poor wear resistance of the titanium alloy are reduced. Therefore, the hybrid implant material shows great potential for reducing material-related aseptic implant loosening after total knee replacement.

Declaration of generative AI in scientific writing

During the preparation of this work the author(s) used Grammarly and DeepL/write in order to correct typos and grammatical errors. After using this tool/service, the author(s) reviewed and edited the content as needed and take(s) full responsibility for the content of the publication.

Funding

This work was supported by the Federal Ministry of Education and Research BMBF, Germany (grant number: 03XP0279D), which had no role in study design; in the collection, analysis, and interpretation of data; in the writing of the report; and in the decision to submit the article for publication.

CRediT authorship contribution statement

Jan-Oliver Sass: Writing – original draft, Visualization, Validation, Supervision, Project administration, Methodology, Investigation, Formal analysis, Data curation, Conceptualization. **Maeruan Kebbach:** Writing – review & editing, Validation, Methodology, Data curation, Conceptualization. **Cornelia Lork:** Writing – review & editing, Project administration, Funding acquisition, Conceptualization. **Jan Johannsen:** Writing – review & editing, Resources, Methodology, Funding acquisition, Conceptualization. **Markus Weinmann:** Writing – review & editing, Resources, Methodology, Funding acquisition, Conceptualization. **Melanie Stenzel:** Writing – review & editing, Resources, Methodology, Funding acquisition, Conceptualization. **Rainer Bader:** Writing – review & editing, Supervision, Funding acquisition, Conceptualization.

Declaration of competing interest

The authors declare the following financial interests/personal relationships which may be considered as potential competing interests: The authors Jan-Oliver Sass, Jan Johannsen, Maeruan Kebbach, Rainer Bader declare that they have no known competing financial interests or personal relationships that could have appeared to influence the work reported in this paper.

Cornelia Lork reports a relationship with ZM Praezisionsdentaltechnik GmbH that includes: employment. Markus Weinmann reports a relationship with TANIOBIS GmbH that includes: employment. Melanie Stenzel reports a relationship with TANIOBIS GmbH that includes: employment.

Data availability

Data will be made available on request.

Acknowledgments

We would like to thank Christoph Lutter (Department of Orthopaedics, Rostock University Medical Center, Rostock, Germany) for his support in the virtual implantation of the femoral component.

Appendix A. Supplementary data

Supplementary data to this article can be found online at https://doi.org/10.1016/j.jmbbm.2024.106681.

References

Bahraminasab, M., Arab, S., Doostmohammadi, N., 2022a. Cytotoxicity and ion release of functionally graded Al_2O_3- Ti orthopedic biomaterial. JBBBE 54, 103–118. https://doi.org/10.4028/www.scientific.net/JBBBE.54.103.

Bahraminasab, M., Arab, S., Ghaffari, S., 2022b. Osteoblastic cell response to Al2O3-Ti composites as bone implant materials. Bioimpacts : BI 12 (3), 247–259. https://doi.org/10.34172/bi.2021.2330.

Bahraminasab, M., Arab, S., Safari, M., Talebi, A., Kavakebian, F., Doostmohammadi, N., 2021. In vivo performance of Al2O3-Ti bone implants in the rat femur. J. Orthop. Surg. Res. 16 (1), 79. https://doi.org/10.1186/s13018-021-02226-7.

Bahraminasab, M., Bozorg, M., Ghaffari, S., Kavakebian, F., 2019. Electrochemical corrosion of Ti-Al2O3 biocomposites in Ringer's solution. J. Alloys Compd. 777, 34–43. https://doi.org/10.1016/j.jallcom.2018.09.313.

Bahraminasab, M., Ghaffari, S., Eslami-Shahed, H., 2017. Al2O3-Ti functionally graded material prepared by spark plasma sintering for orthopaedic applications. J. Mech. Behav. Biomed. Mater. 72, 82–89. https://doi.org/10.1016/j.jmbbm.2017.04.024.

Bahraminasab, M., Sahari, B.B., Edwards, K.L., Farahmand, F., Hong, T.S., Naghibi, H., 2013. Material tailoring of the femoral component in a total knee replacement to reduce the problem of aseptic loosening. Mater. Des. 52, 441–451. https://doi.org/10.1016/j.matdes.2013.05.066.

Bedir, T., Altan, E., Aranci-Ciftci, K., Gunduz, O., 2023. Bioceramics. In: Gunduz, O., Egles, C., Pérez, R.A., Ficai, D., Ustundag, C.B. (Eds.), Biomaterials and Tissue Engineering, vol. 74. Springer International Publishing, Cham, pp. 175–203.

Bendich, I., Lawrie, C.M., Riegler, V., Barrack, R.L., Nunley, R.M., 2022. The impact of component design and fixation on stress shielding after modern total knee arthroplasty. J. Arthroplasty 37 (6S), S221–S225. https://doi.org/10.1016/j.arth.2022.01.074.

Berahmani, S., Janssen, D., Verdonschot, N., 2017. Experimental and computational analysis of micromotions of an uncemented femoral knee implant using elastic and plastic bone material models. J. Biomech. 61, 137–143. https://doi.org/10.1016/j.jbiomech.2017.07.023.

Berahmani, S., Janssen, D., Wolfson, D., Rivard, K., Waal Malefijt, M. de, Verdonschot, N., 2015. The effect of surface morphology on the primary fixation strength of uncemented femoral knee prosthesis: a cadaveric study. J. Arthroplasty 30 (2), 300–307. https://doi.org/10.1016/j.arth.2014.09.030.

Bergschmidt, P., Ellenrieder, M., Bader, R., Kluess, D., Finze, S., Schwemmer, B., Mittelmeier, W., 2016. Prospective comparative clinical study of ceramic and metallic femoral components for total knee arthroplasty over a five-year follow-up period. Knee 23 (5), 871–876. https://doi.org/10.1016/j.knee.2016.06.001.

Carter, D.R., Fyhrie, D.P., Whalen, R.T., 1987. Trabecular bone density and loading history: regulation of connective tissue biology by mechanical energy. J. Biomech. 20 (8), 785–794. https://doi.org/10.1016/0021-9290(87)90058-3.

Crutsen, J.R.W., Koper, M.C., Jelsma, J., Heymans, M., Heyligers, I.C., Grimm, B., Mathijssen, N.M.C., Schotanus, M.G.M., 2022. Prosthetic hip-associated cobalt toxicity: a systematic review of case series and case reports. EFORT open reviews 7 (3), 188–199. https://doi.org/10.1530/EOR-21-0098.

Drynda, A., Drynda, S., Kekow, J., Lohmann, C.H., Bertrand, J., 2018. Differential effect of cobalt and chromium ions as well as CoCr particles on the expression of osteogenic markers and osteoblast function. Int. J. Mol. Sci. 19 (10) https://doi.org/10.3390/ijms19103034.

Eisenbarth, E., Velten, D., Müller, M., Thull, R., Breme, J., 2004. Biocompatibility of beta-stabilizing elements of titanium alloys. Biomaterials 25 (26), 5705–5713. https://doi.org/10.1016/j.biomaterials.2004.01.021.

Farrahnoor, A., Zuhailawati, H., 2021. Review on the mechanical properties and biocompatibility of titanium implant: the role of niobium alloying element. Int. J. Mater. Res. 112 (6), 505–513. https://doi.org/10.1515/ijmr-2020-8060.

Fregly, B.J., Besier, T.F., Lloyd, D.G., Delp, S.L., Banks, S.A., Pandy, M.G., D'Lima, D.D., 2012. Grand challenge competition to predict in vivo knee loads. J. Orthop. Res. : official publication of the Orthopaedic Research Society 30 (4), 503–513. https://doi.org/10.1002/jor.22023.

Galas, A., Banci, L., Innocenti, B., 2023. The effects of different femoral component materials on bone and implant response in total knee arthroplasty: a finite element analysis. Materials 16 (16). https://doi.org/10.3390/ma16165605.

Gao, X., Fraulob, M., Haïat, G., 2019. Biomechanical behaviours of the bone-implant interface: a review. J. R. Soc., Interface 16 (156), 20190259. https://doi.org/10.1098/rsif.2019.0259.

Godest, A.C., Beaugonin, M., Haug, E., Taylor, M., Gregson, P.J., 2002. Simulation of a knee joint replacement during a gait cycle using explicit finite element analysis. J. Biomech. 35 (2), 267–275. https://doi.org/10.1016/S0021-9290(01)00179-8.

Grimberg, A., Lützner, J., Melsheimer, O., Morlock, M., Steinbrück, A., 2023. Arthroplasty Register Germany (EPRD) - Annual Report 2023: Mit Sicherheit Mehr Qualität. EPRD Deutsche Endoprothesenregister, Berlin, p. 175.

Huiskes, R., Weinans, H., Grootenboer, H.J., Dalstra, M., Fudala, B., Slooff, T.J., 1987. Adaptive bone-remodeling theory applied to prosthetic-design analysis. J. Biomech. 20 (11–12), 1135–1150. https://doi.org/10.1016/0021-9290(87)90030-3.

Järvenpää, J., Soininvaara, T., Kettunen, J., Miettinen, H., Kröger, H., 2014. Changes in bone mineral density of the distal femur after total knee arthroplasty: a 7-year DEXA follow-up comparing results between obese and nonobese patients. Knee 21 (1), 232–235. https://doi.org/10.1016/j.knee.2013.03.004.

Johannsen, J., Lauhoff, C., Stenzel, M., Schnitter, C., Niendorf, T., Weinmann, M., 2023. Laser beam powder bed fusion of novel biomedical titanium/niobium/tantalum alloys: powder synthesis, microstructure evolution and mechanical properties. Mater. Des. 233, 112265 https://doi.org/10.1016/j.matdes.2023.112265.

Jonitz-Heincke, A., Sellin, M.-L., Seyfarth, A., Peters, K., Mueller-Hilke, B., Fiedler, T., Bader, R., Klinder, A., 2019. Analysis of cellular activity short-term exposure to cobalt and chromium ions in mature human osteoblasts. Materials 12 (17). https://doi.org/10.3390/ma12172771.

Kaur, M., Singh, K., 2019. Review on titanium and titanium based alloys as biomaterials for orthopaedic applications. Materials science & engineering. C, Materials for biological applications 102, 844–862. https://doi.org/10.1016/j.msec.2019.04.064.

Kebbach, M., Darowski, M., Krueger, S., Schilling, C., Grupp, T.M., Bader, R., Geier, A., 2020. Musculoskeletal multibody simulation analysis on the impact of patellar component design and positioning on joint dynamics after unconstrained total knee arthroplasty. Materials 13 (10). https://doi.org/10.3390/ma13102365.

Kebbach, M., Geier, A., Darowski, M., Krueger, S., Schilling, C., Grupp, T.M., Bader, R., 2023. Computer-based analysis of different component positions and insert thicknesses on tibio-femoral and patello-femoral joint dynamics after cruciate-retaining total knee replacement. Knee 40, 152–165. https://doi.org/10.1016/j.knee.2022.11.010.

Keyak, J.H., Falkinstein, Y., 2003. Comparison of in situ and in vitro CT scan-based finite element model predictions of proximal femoral fracture load. Med. Eng. Phys. 25 (9), 781–787. https://doi.org/10.1016/S1350-4533(03)00081-X.

Kluess, D., Bergschmidt, P., Mueller, I., Mittelmeier, W., Bader, R., 2012. Influence of the distal femoral resection angle on the principal stresses in ceramic total knee components. Knee 19 (6), 846–850. https://doi.org/10.1016/j.knee.2012.03.014.

Kluess, D., Mittelmeier, W., Bader, R., 2010. Intraoperative impaction of total knee replacements: an explicit finite-element-analysis of principal stresses in ceramic vs. cobalt-chromium femoral components. Clin. Biomech. 25 (10), 1018–1024. https://doi.org/10.1016/j.clinbiomech.2010.08.002.

Krueger, A.P., Singh, G., Beil, F.T., Feuerstein, B., Ruether, W., Lohmann, C.H., 2014. Ceramic femoral component fracture in total knee arthroplasty: an analysis using fractography, fourier-transform infrared microscopy, contact radiography and histology. J. Arthroplasty 29 (5), 1001–1004. https://doi.org/10.1016/j.arth.2013.11.003.

Lee, D.W., Du Ro, H., Han, H.-S., Lee, M.C., 2023. Titanium alloy knee implant is associated with higher bone density over cobalt chromium: a prospective matched-pair case-control study. Clinics in orthopedic surgery 15 (4), 581–588. https://doi.org/10.4055/cios22082.

Luo, J.P., Sun, J.F., Huang, Y.J., Zhang, J.H., Zhang, Y.D., Zhao, D.P., Yan, M., 2019. Low-modulus biomedical Ti-30Nb-5Ta-3Zr additively manufactured by Selective Laser Melting and its biocompatibility. Materials science & engineering. C, Materials for biological applications 97, 275–284. https://doi.org/10.1016/j.msec.2018.11.077.

Mauck, J., Wieding, J., Kluess, D., Bader, R., 2016. Numerical simulation of mechanically stimulated bone remodelling. Current Directions in Biomedical Engineering 2 (1), 643–647. https://doi.org/10.1515/cdbme-2016-0141.

Meneghini, R.M., Mont, M.A., Backstein, D.B., Bourne, R.B., Dennis, D.A., Scuderi, G.R., 2015. Development of a modern knee society radiographic evaluation system and methodology for total knee arthroplasty. J. Arthroplasty 30 (12), 2311–2314. https://doi.org/10.1016/j.arth.2015.05.049.

Mick, E., Tinschert, J., Mitrovic, A., Bader, R., 2015. A novel technique for the connection of ceramic and titanium implant components using glass solder bonding. Materials 8 (7), 4287–4298. https://doi.org/10.3390/ma8074287.

Mintzer, C.M., Robertson, D.D., Rackemann, S., Ewald, F.C., Scott, R.D., Spector, M., 1990. Bone loss in the distal anterior femur after total knee arthroplasty. Clin. Orthop. Relat. Res. 260, 135–143.

Moayedee, Y., Nikzad, L., Majidian, H., 2024. Exploration into the microstructural, mechanical, and biological characteristics of the functionally graded 3Y-TZP/Ti6Al4V system as a potential material for dental implants. J. Mech. Behav. Biomed. Mater. 151, 106380 https://doi.org/10.1016/j.jmbbm.2024.106380.

Ni, J., Ling, H., Zhang, S., Wang, Z., Peng, Z., Benyshek, C., Zan, R., Miri, A.K., Li, Z., Zhang, X., Lee, J., Lee, K.-J., Kim, H.-J., Tebon, P., Hoffman, T., Dokmeci, M.R., Ashammakhi, N., Li, X., Khademhosseini, A., 2019. Three-dimensional printing of metals for biomedical applications. Materials today. Bio 3, 100024. https://doi.org/10.1016/j.mtbio.2019.100024.

Niinomi, M., 1998. Mechanical properties of biomedical titanium alloys. Mater. Sci. Eng. 243 (1–2), 231–236. https://doi.org/10.1016/S0921-5093(97)00806-X.

Ozan, S., Lin, J., Li, Y., Wen, C., 2017. New Ti-Ta-Zr-Nb alloys with ultrahigh strength for potential orthopedic implant applications. J. Mech. Behav. Biomed. Mater. 75, 119–127. https://doi.org/10.1016/j.jmbbm.2017.07.011.

Pilz, S., Gustmann, T., Günther, F., Zimmermann, M., Kühn, U., Gebert, A., 2022. Controlling the Young's modulus of a ß-type Ti-Nb alloy via strong texturing by LPBF. Mater. Des. 216, 110516 https://doi.org/10.1016/j.matdes.2022.110516.

Post, C.E., Bitter, T., Briscoe, A., Verdonschot, N., Janssen, D., 2022. A FE study on the effect of interference fit and coefficient of friction on the micromotions and interface gaps of a cementless PEEK femoral component. J. Biomech. 137, 111057 https://doi.org/10.1016/j.jbiomech.2022.111057.

Rho, J.Y., Hobatho, M.C., Ashman, R.B., 1995. Relations of mechanical properties to density and CT numbers in human bone. Med. Eng. Phys. 17 (5), 347–355. https://doi.org/10.1016/1350-4533(95)97314-f.

Roulet, J.-F., Schepker, K.L., Truco, A., Schwarz, H.-C., Rocha, M.G., 2021. Biaxial flexural strength, crystalline structure, and grain size of new commercially available zirconia-based ceramics for dental appliances produced using a new slip-casting method. J. Mech. Behav. Biomed. Mater. 114, 104180 https://doi.org/10.1016/j.jmbbm.2020.104180.

Ruiter, L. de, Janssen, D., Briscoe, A., Verdonschot, N., 2017. The mechanical response of a polyetheretherketone femoral knee implant under a deep squatting loading condition. Proceedings of the Institution of Mechanical Engineers. Part H. Journal of engineering in medicine 231 (12), 1204–1212. https://doi.org/10.1177/0954411917738805.

Ruiter, L. de, Rankin, K., Browne, M., Briscoe, A., Janssen, D., Verdonschot, N., 2021. Decreased stress shielding with a PEEK femoral total knee prosthesis measured in validated computational models. J. Biomech. 118, 110270 https://doi.org/10.1016/j.jbiomech.2021.110270.

Sass, J.-O., Hembus, J., Fuhrmann, E., Vogel, D., Bauer, E., Link, H.D., Bader, R., 2023. Pre-clinical characterization of a novel flexible surface stem design for total knee replacements. Proceedings of the Institution of Mechanical Engineers. Part H. Journal of engineering in medicine 237 (10), 1154–1166. https://doi.org/10.1177/09544119231197596.

Sass, J.-O., Henke, P., Mitrovic, A., Weinmann, M., Kluess, D., Johannsen, J., Sellin, M.-L., Lembke, U., Reimer, D., Lork, C., Jonitz-Heincke, A., Bader, R., 2024a. Multifunctional hybrid material for endoprosthetic implants based on alumina-toughened zirconia ceramics and additively manufactured TiNbTa alloys. Materials 17 (8), 1838. https://doi.org/10.3390/ma17081838.

Sass, J.-O., Johnson, K., Darques, J.-B., Buerstenbinder, L., Soodmand, I., Bader, R., Kebbach, M., 2024b. Influence of posterior cruciate ligament tension on tibiofemoral and patellofemoral joint contact mechanics in cruciate-retaining total knee replacement: a combined musculoskeletal multibody and finite-element simulation. Computer Methods in Biomechanics and Biomedical Engineering, pp. 1–13. https://doi.org/10.1080/10255842.2024.2329946.

Sass, J.-O., Sellin, M.-L., Kauertz, E., Johannsen, J., Weinmann, M., Stenzel, M., Frank, M., Vogel, D., Bader, R., Jonitz-Heincke, A., 2024c. Advanced Ti–Nb–Ta alloys for bone implants with improved functionality. J. Funct. Biomater. 15 (2), 46. https://doi.org/10.3390/jfb15020046.

Sauer, A., Maas, A., Ottawa, S., Giurea, A., Grupp, T.M., 2021. Towards a new, pre-clinical, subject-independent test model for kinematic analysis after total knee arthroplasty—influence of the proximo-distal patella position and patellar tendon stiffness. Appl. Sci. 11 (21), 10322 https://doi.org/10.3390/app112110322.

Schileo, E., Dall'ara, E., Taddei, F., Malandrino, A., Schotkamp, T., Baleani, M., Viceconti, M., 2008. An accurate estimation of bone density improves the accuracy of subject-specific finite element models. J. Biomech. 41 (11), 2483–2491. https://doi.org/10.1016/j.jbiomech.2008.05.017.

Schulze, C., Weinmann, M., Schweigel, C., Keßler, O., Bader, R., 2018. Mechanical properties of a newly additive manufactured implant material based on Ti-42Nb. Materials 11 (1). https://doi.org/10.3390/ma11010124.

Sequeira, S., Fernandes, M.H., Neves, N., Almeida, M.M., 2017. Development and characterization of zirconia–alumina composites for orthopedic implants. Ceram. Int. 43 (1), 693–703. https://doi.org/10.1016/j.ceramint.2016.09.216.

Song, C., Liu, L., Deng, Z., Lei, H., Yuan, F., Yang, Y., Li, Y., Yu, J., 2023. Research progress on the design and performance of porous titanium alloy bone implants. J. Mater. Res. Technol. 23, 2626–2641. https://doi.org/10.1016/j.jmrt.2023.01.155.

Suansuwan, N., Swain, M.V., 2003. Adhesion of porcelain to titanium and a titanium alloy. J. Dent. 31 (7), 509–518. https://doi.org/10.1016/S0300-5712(03)00071-X.

Sun, Q., Yang, L., Yang, W., Ji, H., Li, M., Li, Y., 2022. Microstructure evolution and bonding mechanism of ZrO2 ceramic and Ti-6Al-4V alloy joints brazed by Bi2O3-B2O3-ZnO glass paste. J. Eur. Ceram. Soc. 42 (13), 5953–5963. https://doi.org/10.1016/j.jeurceramsoc.2022.06.016.

Tischer, T., Geier, A., Lutter, C., Enz, A., Bader, R., Kebbach, M., 2023. Patella height influences patellofemoral contact and kinematics following cruciate-retaining total knee replacement. J. Orthop. Res. : official publication of the Orthopaedic Research Society 41 (4), 793–802. https://doi.org/10.1002/jor.25425.

Uivaraseanu, B., Vesa, C.M., Tit, D.M., Maghiar, O., Maghiar, T.A., Hozan, C., Nechifor, A.C., Behl, T., Andronie-Cioara, F.L., Patrascu, J.M., Bungau, S., 2022. Highlighting the advantages and benefits of cementless total knee arthroplasty. Exp. Ther. Med. 23 (1), 58. https://doi.org/10.3892/etm.2021.10980 (Review).

van Jonbergen, H.-P.W., Innocenti, B., Gervasi, G.L., Labey, L., Verdonschot, N., 2012. Differences in the stress distribution in the distal femur between patellofemoral joint replacement and total knee replacement: a finite element study. J. Orthop. Surg. Res. 7, 28. https://doi.org/10.1186/1749-799X-7-28.

Vásquez, V.Z.C., Ozcan, M., Kimpara, E.T., 2009. Evaluation of interface characterization and adhesion of glass ceramics to commercially pure titanium and gold alloy after

thermal- and mechanical-loading. Dent. Mater. : official publication of the Academy of Dental Materials 25 (2), 221–231. https://doi.org/10.1016/j.dental.2008.07.002.
Vogel, D., Wehmeyer, M., Kebbach, M., Heyer, H., Bader, R., 2021. Stress and strain distribution in femoral heads for hip resurfacing arthroplasty with different materials: A finite element analysis. Journal of the mechanical behavior of biomedical materials 113, 104115. https://doi.org/10.1016/j.jmbbm.2020.104115.
Wolff, J., 2010. The classic: on the theory of fracture healing. 1873. Clin. Orthop. Relat. Res. 468 (4), 1052–1055. https://doi.org/10.1007/s11999-010-1240-9.
Yang, S., Zhang, K., Li, F., Jiang, J., Jia, T., Yang, S.-Y., 2015. Biological responses of preosteoblasts to particulate and ion forms of Co-Cr alloy. J. Biomed. Mater. Res. 103 (11), 3564–3571. https://doi.org/10.1002/jbm.a.35501.
Yilmaz, M., Holm, C.E., Lind, T., Flivik, G., Odgaard, A., Petersen, M.M., 2021. Bone remodeling and implant migration of uncemented femoral and cemented asymmetrical tibial components in total knee arthroplasty - DXA and RSA evaluation with 2-year follow up. Knee surgery & related research 33 (1), 25. https://doi.org/10.1186/s43019-021-00111-5.